IOP Publishing Journal of Physics B: Atomic, Molecular and Optical Physics

J. Phys. B: At. Mol. Opt. Phys. **51** (2018) 045004 (12pp) https://doi.org/10.1088/1361-6455/aaa182

Dielectronic recombination of the open 4*d*-shell of tungsten: W^{37+}–W^{28+}

S P Preval, N R Badnell and M G O'Mullane

Department of Physics, University of Strathclyde, Glasgow G4 0NG, United Kingdom

E-mail: simon.preval@strath.ac.uk

Received 25 October 2017, revised 27 November 2017
Accepted for publication 13 December 2017
Published 24 January 2018

Abstract

Tungsten is an important element for magnetically confined fusion plasmas but has the potential to cool, or even quench the plasma due to it being an efficient radiator. Total and level-resolved dielectronic recombination (DR) rate coefficients, for all ionisation stages, are essential to model tungsten. We describe a set calculations performed using the distorted wave code AUTOSTRUCTURE for the tungsten ions W^{37+}–W^{28+}. We demonstrate the importance of relativistic configuration mixing in such calculations. In particular, we show that the partial DR rate coefficients calculated in level and configuration resolution can differ by as little as 5%, and up to as much as 75%. Using the new data, we calculate a revised steady-state ionisation fraction for tungsten. We find that, relative to the ionisation fraction calculated using the recombination rate coefficients of Putterich *et al* (2008 *Plasma Phys. Control. Fusion* **50** 085016), the peak temperatures of W^{37+}–W^{28+} ionisation states are shifted to lower temperatures spanning 0.9–1.6 keV. This temperature range is important for understanding the performance of large tokamaks, such as ITER, because the temperatures in the pedestal, edge, scrape-off-layer and divertor region fall in this range.

Keywords: dielectronic recombination, electron–ion collisions, finite density plasmas, tungsten

(Some figures may appear in colour only in the online journal)

1. Introduction

The experimental thermonuclear tokamak reactor ITER is currently being built in Cadarache, France, with its first plasma projected to be in 2025. Designed to output 10 times as much energy as it consumes, it is posited to be the penultimate step in realising a commercial fusion reactor. The plasma facing component of the divertor will be coated with tungsten. This metal has been chosen due to its resistance to tritium absorption, its ability to withstand large power loads, and its high melting point. However tungsten will be sputtered into the core, confined, plasma. Tungsten as an impurity in the confined plasma is a problem because it is a very efficient radiator, which will lead to cooling of the plasma, and potentially quenching it. A key method in understanding the impact of tungsten impurities on the tokamak plasma is detailed collisional–radiative modelling [1]. However, such modelling requires the provision of partial, final-state resolved dielectronic/radiative recombination (DR/RR) rate coefficients for the ion being modelled.

High temperatures in the core are required to enable the fusion reaction and maintaining this core temperature necessitates a high temperature at the plasma edge. The pedestal region is characterised by a steep pressure ($p = n_e T_e$) gradient at the edge which forms a transport barrier; maximising its height, and inter alia the edge temperature, is the preferred way to achieve high performance [2]. Unfortunately the plasma conditions of this high confinement (H-mode) regime are susceptible to MHD instabilities which collapse the pedestal, thus reducing the temperature and allowing impurities into the core region, resulting in reduced performance or destruction of the conditions needed to sustain the fusion reaction. Radiation from high efficiency radiators such as tungsten will affect the balance between the competing effects. For ITER the pedestal temperature is 14 keV depending on model and extrapolations from JET ITER-like wall experiments [2, 3]. The ionisation stages of tungsten reported here fall in this region so it is important to be able to model their distribution, particularly in regions like the pedestal, where turbulent transport is strongly suppressed.

Several isonuclear datasets for tungsten have been calculated using a variety of methods. The first was generated by Post *et al* [4, 5] using an average-ion method with the ADPAK codes. Later, Pütterich *et al* [6] used these recombination rate coefficients in modelling the tokamak plasmas from ASDEX upgrade, but scaled several ionisation stages (W^{20+}–W^{55+}) by empirically determined constants to match observed spectral emission. Next, Foster [7] used a combination of the Burgess General Formula [8] and the Burgess–Bethe General Programme [9] to calculate DR rate coefficients for the sequence. The RR rate coefficients were calculated by scaling hydrogenic results. Lastly, there exists a complete set of recombination rate coefficients on the International Atomic Energy Agency website[1] calculated using the FLYCHK code [10], which also uses an average-ion method. Despite the numerous calculations available and the wide range of methods used, poor agreement between the calculated recombination rate coefficients is observed between all three datasets. Examples of this poor agreement can be seen in Kwon *et al* [11], where multiple comparisons are made between these datasets. Clearly, further theoretical investigation is required to resolve this disagreement.

The demand for partial final-state resolved DR rate coefficients for tungsten has seen a surge in the number of calculations being performed. Typically, these calculations covered ions where the outer valence electron shell is full or nearly full, which are useful for plasma diagnostics. Safronova *et al* has calculated DR rate coefficients for a wide range of tungsten ions using the Cowan [12] and HULLAC [13] codes, covering W^{5+}, W^{6+}, W^{28+}, W^{38+}, W^{45+}, W^{46+}, W^{63+}, and W^{64+} [14–21]. Behar *et al* also used the Cowan and HULLAC codes to calculate DR rate coefficients for W^{45+}, W^{46+}, W^{56+}, and W^{64+} [22–24]. The Flexible Atomic Code (FAC) can also calculate DR rate coefficients, and was used by Li *et al* to calculate data for W^{29+}, W^{39+}, W^{27+}, W^{28+}, and W^{64+} [25–27]. In addition, Meng *et al* and Wu *et al* have also used FAC to calculate DR for W^{47+}, and W^{46+}–W^{46+}, respectively. Lastly, Kwon *et al* used FAC to calculate DR rate coefficients for W^{44+}–W^{46+} [28, 29].

Several works are now exploring ions of tungsten where the valence shell is partially or half full. The most complicated example to date is the work of Spruck *et al* and Badnell *et al* [30–32], where the authors compared experimental storage ring measurements of DR for W^{18+}, W^{19+}, and W^{20+} (ground configurations $4f^{10}$, $4f^{9}$, and $4f^{8}$, respectively) with calculations from the atomic collision package AUTOSTRUCTURE [33–35]. Other approaches to dealing with such complex ions include the use of statistical methods such as those employed by Dzuba *et al* [36, 37], Berengut *et al* [38], and Harabati *et al* [39]. An excellent review of the methods used to study 4*f*-shell ions, both experimentally and theoretically, has been compiled by Krantz *et al* [40].

The most recent attempt to cover the entire isonuclear sequence is known informally as *The Tungsten Project*. Using AUTOSTRUCTURE, Preval *et al* has calculated DR and RR rate coefficients for W^{73+}–W^{38+} [41, 42]. Because of the increased activity in calculating data for tungsten, multiple comparisons have been performed with data from *The Tungsten Project*, confirming the reliability of the calculation methods used. All data from these publications have been published on the OPEN-ADAS website[2] in the standard adf09 (DR) and adf48 (RR) formats. The definitions of these formats can also be found on the OPEN-ADAS website.

While not as complicated as the open 4*f* shell, calculating DR rate coefficients for open 4*d* shell ions still represents a significant jump in complexity to ions considered previously. The rich level structure of these ions also presents interesting physics in its own right. It is for this reason that this paper is dedicated to the $4d^q$ ($q = 1$–10) isonuclear sequence of tungsten, covering charge states W^{37+}–W^{28+}. As in Preval *et al* [41, 42] we use some technical notation when discussing the various ionisation stages. Beyond Zn-like, referring to ions by their isoelectronic chemical symbol requires a good memory of the periodic table. It is for this reason that we refer to the various ionisation stages by the number of valence electrons instead. For example, H-like ($Z = 1$) becomes 01-like, and Pd-like ($Z = 46$) with 46 valence electrons becomes 46-like.

We structure this paper as follows. We first describe the underlying theory for our DR calculations. Next, we present and discuss our results, and compare our DR rate coefficients to those calculated in other works. Finally, we assess the quantitative effect of using our data in calculating the steady-state ionisation fraction for tungsten, and demonstrate how the $4d^q$ ions can be potentially used as a temperature diagnostic. We conclude with a few remarks.

2. Theory

The theory underpinning the calculation of DR rate coefficients has been discussed at length in multiple works, however, we summarise the basic principles here. All DR rate coefficients described in this paper were calculated using the distorted wave code AUTOSTRUCTURE. It is able to calculate energy levels, radiative/autoionization rates, collision strengths, and many other quantities. The code is able to calculate data in configuration average (CA), term (LS), or level (IC) resolution using relativistic κ-averaged wavefunctions. AUTOSTRUCTURE has been benchmarked extensively against experimental DR measurements for various ions such as Fe^{19+} [43], and F^{5+} [44].

For an ion $X_\nu^{(+z+1)}$ with residual charge z in an initial state ν recombining into an ion X_f^{+z} with final state f, the partial DR rate coefficient ${}^{\mathrm{DR}}\alpha_{f\nu}^{z+1}$ at a particular electron

[1] https://amdis.iaea.org/FLYCHK/

[2] http://open.adas.ac.uk

Table 1. Example configuration set for the 40-like 4–4 core excitation. Configurations marked with an * are mixing configurations as determined by the one-up one down rule.

N-electron	$(N+1)$-electron
$4p^6 4d^4$	$4p^6 4d^5$
$4p^6 4d^3 4f$	$4p^6 4d^4 4f$
$4p^5 4d^5$	$4p^6 4d^3 4f^2$
$4p^5 4d^4 4f$	$4p^5 4d^6$
$4p^6 4d^2 4f^2$*	$4p^5 4d^5 4f$
$4p^4 4d^6$*	$4p^5 4d^4 4f^2$
	$4p^4 4d^7$*
	$4p^4 4d^6 4f$*
	$4p^6 4d^2 4f^3$*

temperature, T_e, can be written as

$$^{\mathrm{DR}}\alpha_{f\nu}^{z+1}(T_e) = \left(\frac{4\pi a_0^2 I_H}{k_B T_e}\right)^{\frac{3}{2}} \sum_j \frac{\omega_j}{2\omega_\nu} \exp\left[-\frac{E}{k_B T_e}\right] \times \frac{\sum_l A^a_{j\to\nu,E\,l} A^r_{j\to f}}{\sum_h A^r_{j\to h} + \sum_{m,l} A^a_{j\to m,E\,l}}, \quad (1)$$

where ω_ν and ω_j are the statistical weights of the N- and $(N+1)$-electron–ions, respectively, the A^r and A^a are the radiative and Auger rates, respectively, and E is the total energy of the continuum electron minus its rest energy, which is fixed by the position of the resonances. The sum over l is performed over all orbital angular momentum quantum numbers included, and the sum over j is over all autoionizing levels. The sums over h and m give the total radiative and Auger widths, respectively. Lastly, I_H is the ionisation energy of the hydrogen atom, k_B is the Boltzmann constant, and $(4\pi a_0^2)^{3/2} = 6.6011 \times 10^{-24}$ cm^3.

The RR rate coefficients for the $4d$ ions are now completely overwhelmed by the DR rate coefficients. Therefore, they are calculated for *The Tungsten Project* for completeness only. RR contributes at most $\sim$4% for 37-like at peak abundance temperature (2.7×10^7 K), decreasing to $\sim$1% for 46-like at peak abundance temperature (2.7×10^7 K). The RR rate coefficient $^{\mathrm{RR}}\alpha_{f\nu}^{z+1}(T_e)$ can be written in terms of its inverse, photoionization $^{\mathrm{PI}}\sigma_{\nu f}^{z}(E)$, using detailed balance. Therefore, the partial RR rate coefficient can be written as:

$$^{\mathrm{RR}}\alpha_{f\nu}^{z+1}(T_e) = \frac{c\,\alpha^3}{\sqrt{\pi}} \frac{\omega_f}{2\omega_\nu} (I_H k_B T_e)^{-3/2} \times \int_0^\infty E_{\nu f}^2\, {}^{\mathrm{PI}}\sigma_{\nu f}^{z}(E) \exp\left[-\frac{E}{k_B T_e}\right] \mathrm{d}E, \quad (2)$$

where $E_{\nu f}$ is the corresponding photon energy, and $c\,\alpha^3/\sqrt{\pi} = 6572.67$ cm s^{-1}.

At high energies and temperatures, relativistic effects must be factored into the Maxwell–Boltzmann distribution. This results in a correction factor to the distribution giving the Maxwell–Jüttner distribution [45], which can be written as:

$$F_r(\theta) = \sqrt{\frac{\pi\theta}{2}} \frac{1}{K_2(1/\theta)\mathrm{e}^{1/\theta}}, \quad (3)$$

where $\theta = \alpha^2 k_B T/2I_H$, α is the fine-structure constant and K_2 is the modified Bessel function of the second kind. As we move along the isonuclear sequence the Jüttner correction becomes less relevant. For the $4d$ ions considered in the present work, the Jüttner correction causes a change of <1% at peak abundance for 37-like, and even less for 46-like. However, the high-temperature DR decreases by as much as 50% for 37-like at 2.74×10^9 K, and 35% for 46-like at 1.57×10^9 K.

3. Calculations

3.1. DR

We split our DR rate coefficient calculations into core excitations, which are labelled in terms of the initial and final principal quantum numbers n and n' of the promoted target electron. The largest contributions to the total DR rate coefficient by far come from the outer shell $\Delta n = 0, 1$ core excitations 4–4 and 4–5. In the case of the inner shell $\Delta n = 1$ core excitation (3–4), the filling of the $n = 4$ shell restricts the number of promotions that can occur from $n = 3$, decreasing its importance. The converse is true for the outer shell $\Delta n = 2$ core excitation (4–6).

The 3–4 core excitation was calculated in CA due to its small contribution to the recombination rate coefficient total. The N-electron configuration set included all possible double excitations of 3ℓ and 4ℓ electrons from the ground configuration of the ion considered. The $(N+1)$-electron configurations consisted of all possible triple excitations of 3ℓ and 4ℓ electrons from the ground configuration of the $(N+1)$-electron–ion.

The 4–6 core excitation was also calculated in CA due to its small contribution to the recombination rate coefficient total. The N-electron configuration set was constructed in a similar manner to the 3–4 core excitation, and included all possible double excitations of the 4ℓ electrons from the ground configuration to 5ℓ and 6ℓ. The $(N+1)$-electron configurations included all possible triple excitations of the 4ℓ electrons from the $(N+1)$ ground configuration to 6ℓ.

The 4–4 core excitation was calculated in IC due to its large contribution to the recombination rate coefficient total. The N-electron configurations consisted of single promotions from $4p$ and $4d$ to 4ℓ from the ground configuration of the ion being considered. Promotions from $4s$ were omitted due to their small contribution to the DR rate coefficient total. Mixing configurations were included by way of the 'one-up one-down' rule as described in Cowan's book [12]. For example, for a particular configuration $4p^\mu 4d^\nu 4f^\rho$ the corresponding mixing configurations would be:

- $4p^{\mu-1}4d^{\nu+2}4f^{\rho-1}$,
- $4p^{\mu+1}4d^{\nu-2}4f^{\rho+1}$.

The $(N+1)$-electron configurations consisted of the N-electron configurations with an additional target electron added. We demonstrate the resulting configuration set for 40-like in table 1. Given such a set of configurations, AUTOSTRUCTURE

calculates all possible autoionization and electric dipole radiative rates between them.

The 4–5 core excitation was also calculated in IC. The N-electron configuration set included promotions from $4p$ and $4d$ to 4ℓ and 5ℓ. As with 4–4, promotions from $4s$ were omitted due to their negligible contribution to the total. Mixing configurations were included as described above. The 4–5 core excitation was the most computationally demanding calculation due to the large number of levels. To make the calculations tractable, promotions from $4p$ were omitted from 40- to 43-like, while 'one-up one-down' mixing configurations were omitted from 39- and 45-like. As with 4–4, the $(N+1)$-electron configuration set is just the N-electron configuration set plus an additional target electron.

For each core excitation, DR from Rydberg $n\ell$ electrons were calculated sequentially up to $n = 25$, and then on a quasi-logarithmic grid of n values up to $n = 999$. Interpolation was used to obtain the intermediate n values. We included sufficiently many ℓ values so as to numerically converge the total DR rate coefficient to $<1\%$ over the entire ADAS temperature range, spanning $z^2(10\text{–}10^7)$ K. The number of ℓ values required to achieve numerical convergence varies according to the ionisation state, and the core excitation considered. The maximum required was for 41-like 4–4 with $\ell = 15$.

3.2. RR

RR is most important in the case of highly charged ions. For example, in the case of 02-like tungsten, RR contributes 100% of the recombination rate total at peak abundance temperature (see [41]). In the present work, we have calculated total RR rate coefficients including contributions for dipole radiation only. This is because higher-order multipolar radiation contributions are manifest at high energies, and hence only higher ionisation states of tungsten. Omission of these contributions leads to a change in the total recombination rate coefficient of $\ll 1\%$ for 37-like at peak abundance temperature. Our N-electron configurations consisted of $4d^q$ and $4d^{q-1}4f$ $(q = 1 - 10)$. The $(N+1)$-electron configurations were just the N-electron configurations plus an additional Rydberg electron. As with DR, RR contributions from Rydberg nl electrons were calculated sequentially up to $n = 25$, and then quasi-logarithmically up to $n = 999$, with interpolation being used to obtain the intermediate values. The Rydberg RR was calculated for sufficiently many ℓ values so as to numerically converge the RR rate coefficient to $<1\%$ over the ADAS temperature range. Given its small importance to the calculations, we will not discuss RR any further in this paper.

4. Results

We have calculated level- and configuration-resolved DR rate coefficients for 37- to 46-like tungsten. We split our discussion with respect to the core excitations that have been calculated.

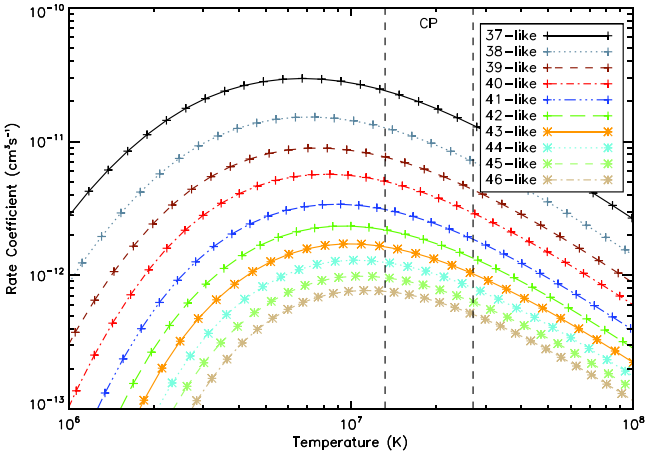

Figure 1. Total DR rate coefficients for the 3–4 core excitation for 37- to 46-like, calculated in CA.

4.1. 3–4

The 3–4 core excitation has been calculated in configuration average, and has been included for completeness. In figure 1 we have plotted the total 3–4 DR rate coefficients for 37- to 46-like. We have also plotted two vertical lines on this figure labelled 'CP' (collisionally ionised plasma). This range is defined as being the range of temperatures going from the peak abundance temperature of 37-like, down to the peak abundance temperature of 46-like. Note that the actual range of temperatures of interest will be wider than this. It can be easily seen that the total DR rate coefficient decreases steadily as more $4d$ electrons are added. As the $4d$ shell is filled, fewer $3p \rightarrow 4d$ electric dipole transitions can take place, decreasing the overall total. For 37-like 3–4 contributes $\sim$15% to the total for temperatures $>3 \times 10^8$ K, but only $\sim$12% at peak abundance temperature (2.7×10^7 K). As we move along the isonuclear sequence, this contribution rapidly drops to $<1\%$ of the total recombination rate coefficient by 46-like at peak abundance.

4.2. 4–4

4–4 is the largest contributor to the total recombination rate coefficient, constituting roughly two thirds of the total for all of the $4d^q$ ions. An example of the configurations included for the 4–4 core excitation is given for 40-like in table 1. In figure 2 we have plotted the total 4–4 DR rate coefficient for 37- to 46-like calculated in IC. As with 3–4, we indicate the range of peak abundances for these ions with the CP region limited by two vertical dashed lines. Very little variation is seen in the DR rate coefficient in the CP region implying insensitivity to the atomic structure of the problem. For 37-like, 4–4 contributes $\sim$60% at peak abundance temperature (2.7×10^7 K). As the $4d$ shell fills, the 4–4 contribution increases to 73% at peak abundance temperature (2.3×10^7 K) for 40-like. By 43-like, 4–4 contributes 76% to the total recombination rate coefficient at peak abundance temperature (1.8×10^7 K). Lastly, by 46-like, the 4–4 contribution decreases slightly, contributing $\sim$70% at peak abundance temperature (1.3×10^7 K) to the total. The total CA DR rate coefficients for the 4–4 core

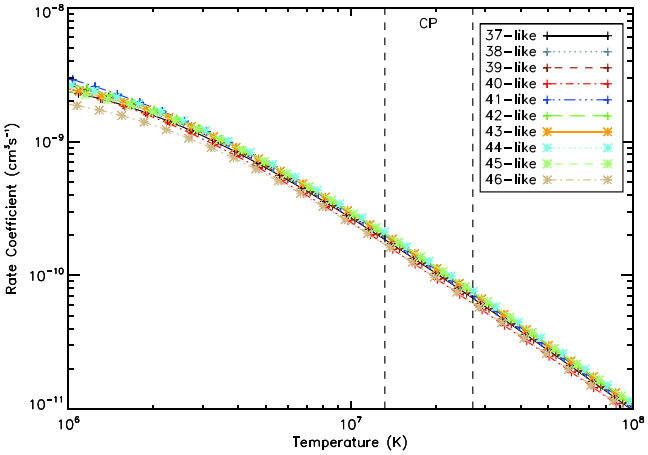

Figure 2. Total DR rate coefficients for the 4–4 core excitation for 37- to 46-like, calculated in IC.

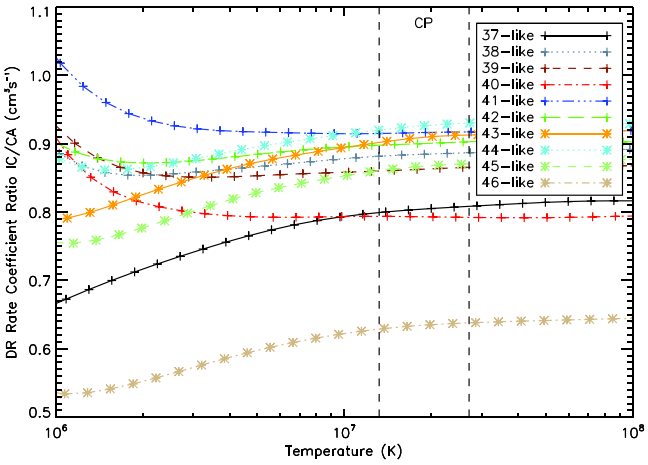

Figure 3. Ratio of the total IC DR rate coefficients for 4–4 to the CA rate coefficients.

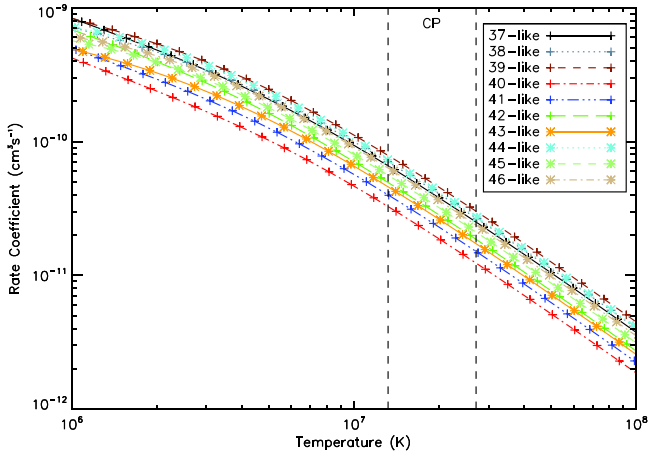

Figure 4. Total DR rate coefficients for the 4–5 core excitation for 37- to 46-like, calculated in IC.

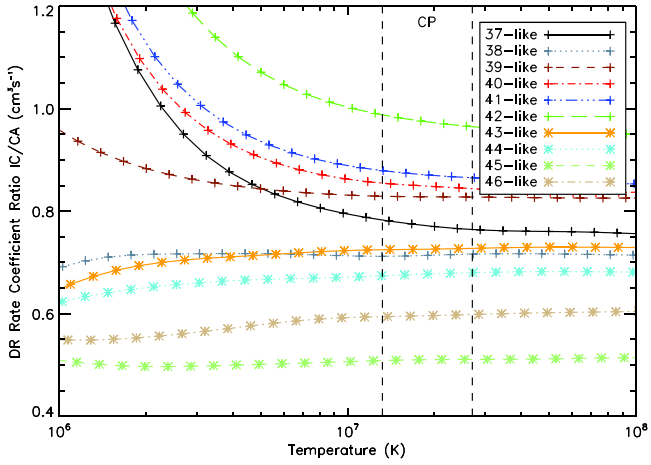

Figure 5. Ratio of the total IC DR rate coefficients for 4–5 to the CA rate coefficients.

excitation are quite similar to their IC counterparts in that they do not change much between different 4*d* ions. Therefore, instead of plotting the CA totals, we opt to plot the ratio of the IC results to the CA results in figure 3. It can be seen that the ratio deviates strongly from unity in the CP region for all ions. This deviation becomes even larger towards low temperatures.

4.3. 4–5

The 4–5 core excitation is the second largest contributor to the total recombination rate coefficient. In figure 4 we have plotted the total 4–5 DR rate coefficients calculated in IC. As with figure 1, we have indicated the CP region with two vertical dashed lines. For 37-like, 4–5 contributes ∼20% at peak abundance temperature. As we move along the iso-nuclear sequence, this contribution fluctuates slightly, ranging from a minimum of 15% for 40-like at peak temperature, to a maximum of 30% for 39-like. For 46-like, 4–5 contributes 25% at peak abundance temperature.

As noted previously, 37-, 38-, and 46-like 4–5 were calculated including contributions from 4*p* and 4*d*, as well as one-up and one-down configurations, and are hence more 'complete' calculations than the other ions. Furthermore, 39-, 44-, and 45-like include contributions from 4*p* and 4*d*, but do not include one-up one-down mixing. Upon close inspection of figure 4 it can be seen that 40-, 41-, 42, and 43-like are separated from the other 4–5 rate coefficient curves. In addition, despite 37-, 38-, and 46-like including one-up one-down mixing, these DR rate coefficients have similar values in the CP region to those excluding these mixing configurations. This implies that the dominant mixing effect on the total 4–5 DR rate coefficient comes from the mixing of single 4*p* and 4*d* promotions, rather than the double promotions from one-up one-down mixing.

As with 4–4, the CA DR rate coefficients are quite similar for all of the 4*d* ions, making comparison with their IC counterparts difficult. In figure 5 we have plotted the ratio of the IC results to the CA results for the 4–5 core excitation. Again, large deviations are seen towards low temperatures.

4.4. 4–6

As with 3–4, the 4–6 core excitation has been calculated in CA only. 4–6 contributes very little to the total recombination

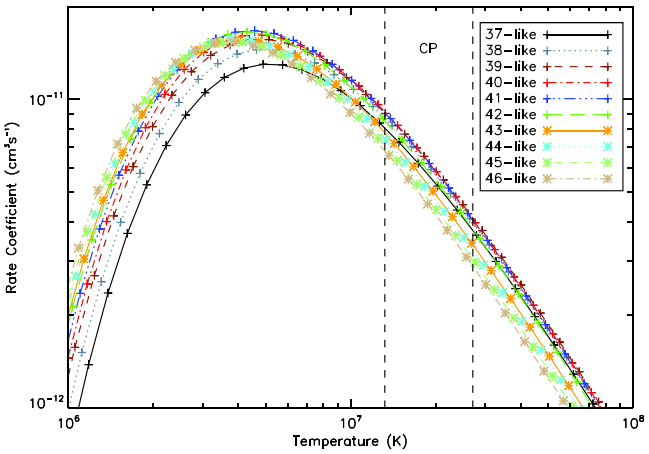

Figure 6. Total DR rate coefficients for the 4–6 core excitation for 37- to 46-like, calculated in CA.

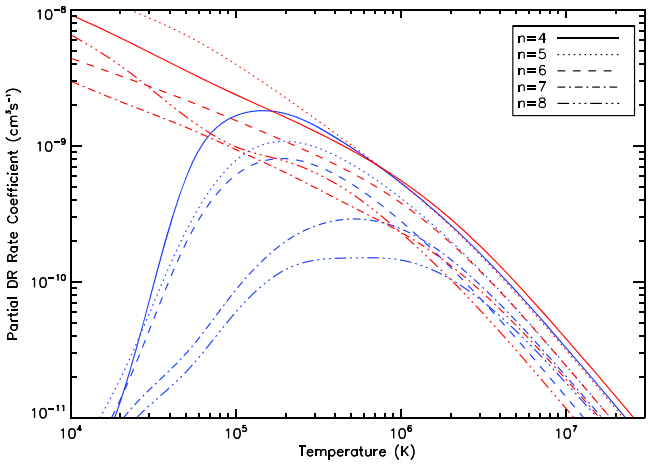

Figure 7. Plot of partial DR rate coefficients for the 4–4 core excitation for 42-like for recombination into n= 4, 5, 6, 7, and 8, calculated in IC (red curves) and CA (blue curves).

Table 2. Comparison of total DR rate coefficients for 41-like 4–4 calculated in IC with ground state shifts of 0, 0.01, and 0.10 Ryd. Note $[x] = 10^x$.

Temp (K)	No shift	Shift 0.01	Shift 0.10
1.09[4]	4.15[−8]	3.78[−8]	4.41[−8]
2.18[4]	2.77[−8]	2.63[−8]	2.74[−8]
5.45[4]	1.67[−8]	1.63[−8]	1.65[−8]
1.09[5]	1.20[−8]	1.19[−8]	1.20[−8]
2.18[5]	7.93[−9]	7.88[−9]	7.87[−9]
5.44[5]	4.29[−9]	4.28[−9]	4.26[−9]
1.09[6]	2.81[−9]	2.80[−9]	2.80[−9]
2.18[6]	1.66[−9]	1.66[−9]	1.66[−9]
5.44[6]	6.28[−10]	6.27[−10]	6.25[−10]
1.09[7]	2.57[−10]	2.57[−10]	2.56[−10]
2.18[7]	9.81[−11]	9.80[−11]	9.75[−11]
5.44[7]	2.57[−11]	2.57[−11]	2.56[−11]
1.09[8]	9.09[−12]	9.09[−12]	9.05[−12]
2.18[8]	3.13[−12]	3.13[−12]	3.12[−12]
5.44[8]	7.23[−13]	7.23[−13]	7.19[−13]
1.09[9]	2.20[−13]	2.20[−13]	2.19[−13]
2.18[9]	5.98[−14]	5.97[−14]	5.94[−14]

rate coefficient, and is just included for completeness. 4–6 constitutes just 3% for 37- and 46-like at peak abundance temperature. We have plotted the total 4–6 DR rate coefficients for 37- to 46-like in figure 6. Little variation is seen for 37- to 46-like in terms of the peak temperature, which ranges from 4 to 5 $\times$ 10^6 K.

5. DR threshold sensitivity

The density and positioning of resonances near threshold can have drastic effects on the DR rate coefficient at low temperatures. If the density of resonances is sufficiently large, then the low temperature DR rate coefficient becomes insensitive to shifts around the threshold. To demonstrate this, we considered the case of 41-like for the 4–4 core excitation. We shifted the ground state of 41-like (ionisation limit of 42-like) by 0.01, and then by 0.1 Ryd. This lowers all resonance positions. Then we compared the resultant total DR rate coefficients to the unshifted case. We have tabulated these DR rate coefficients in table 2. It can be seen that despite these shifts, the total DR rate coefficients vary only slightly by 6%–10% at the lowest temperature considered. While not shown in the present paper, we have checked the sensitivity of the level-resolved DR rate coefficient to shifts at low temperature for all 4d ions. For 38-, and 44- to 46-like, we found that under the 0.1 Ryd shift the DR rate coefficient for the lowest temperatures differs from the unshifted value by 33%–88%. For 37-, and 39-43-like, the difference under the 0.1 Ryd shift is much smaller, with the lowest temperature DR rate coefficient differing by 0%–15% from the unshifted value.

6. Relativistic configuration mixing

As mentioned in the introduction Badnell *et al* [46] considered the effect of mixing in 4d-shell ions of tin, presenting the case of Sn^{10+} as an example. They compared three line strength calculations for Sn^{10+}, calculated including promotions for 4p–4d only, 4d–4f only, and 4p–4d and 4d–4f promotions together. The combined case produced significantly larger line strengths than the individual promotion cases. Mixing is consistent across isoelectronic sequences, meaning that mixing effects observed in tin ions will also be observed in tungsten ions. As seen in sections 4.2 and 4.3 the ratio of the IC to CA DR rate coefficients for the 4–4 and 4–5 core excitations differed greatly from unity, indicating strong mixing effects. This can be more easily seen through consideration of the partial DR rate coefficients. We consider the case of the 4–4 core excitation for 42-like, and examine recombination into n = 4, 5, 6, 7, and 8 in both IC and CA. We plot these rate coefficients in figure 7.

In all cases it can be seen that the IC and CA results diverge at low temperatures. This is simply due to the lack of resonances at threshold in the CA calculation. We focus our

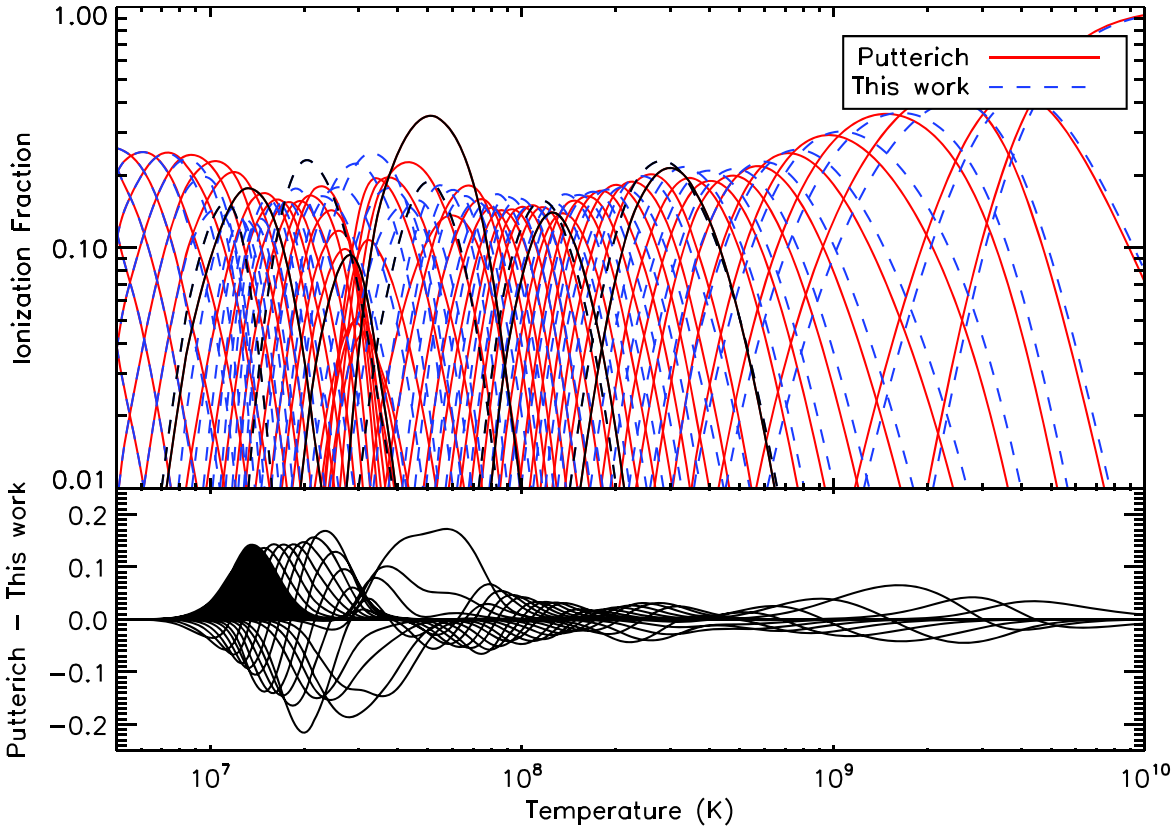

Figure 8. Plot of the zero density ionisation fractions for tungsten. The red-solid fraction was calculated using the recombination rate coefficients of Pütterich *et al* [6], and the ionisation rate coefficients of Loch *et al* [47]. The blue-dashed fraction was calculated in the same way, but the recombination rate coefficient data for 00- to 46-like was replaced with our data from the present work, and Preval *et al* [41, 48]. From right to left, the black parabolas indicate the 10-, 18-, 28-, 36-, and 46-like ionisation fractions.

discussion on temperatures $>1 \times 10^6$ K. The smallest differences between the IC and CA partials are observed for recombination into $n = 4$ and $n = 7$. The $n = 4$ IC partial is larger than the CA partial by 18%, while the $n = 7$ IC partial is smaller than its CA counterpart by 4%. For recombination into $n = 5$ and 6, the IC partial is larger than the CA partial by 30% and 75%, respectively. Lastly, for recombination into $n = 8$, the IC partial is smaller than its CA counterpart by 42%.

7. Ionisation balance

We now consider the impact of our calculations on the coronal-approximation ionisation fraction of tungsten. We consider this approximation for simplicity. This is done by first calculating the ionisation fraction using the recombination rate coefficients of Pütterich *et al* [6] and the ionisation rate coefficients of Loch *et al* [47]. We then compare this with a similar calculation, where we replace the DR+RR rate coefficients with the values reported here. We plot the two ionisation fractions in figure 8, along with the arithmetic difference between the Pütterich *et al* and current ionisation fractions. Note that for our discussion of these ionisation fractions, we have omitted the Jüttner correction described in section 2.

The most striking result emerging from this plot is the close grouping of the peak abundance temperatures for the 4*d* ions. In the present ionisation fractional abundance, the envelope of peak temperatures is 0.97–1.6 keV for 46- to 37-like, whereas in the Pütterich *et al* ionisation fraction, the same stages peak at higher temperatures and cover a wider range, 1.1–2.3 keV. The new rates result in a significant narrowing of the fractional abundances, almost by a factor of 2 at the FWHM value. The stages adjacent to this group, 47-like to 50-like, also show a narrowing effect (at a smaller 20% level) which shows the influence of neighbouring ionisation stages.

In addition, the peak fraction using our data ranges from 0.13 to 0.17, whereas the Pütterich *et al* peak fraction ranges from 0.1 to 0.2. The consistency of the peak fraction and the narrow temperature range in which the 4*d*-shell ions are most abundant can potentially offer an accurate plasma diagnostic. Observation of spectral emission originating from a 4*d* ion would tightly constrain the temperature of the originating plasma. The temperature region of these ionisation stages will be of particular interest to the fusion community as the pedestal temperature at ITER is expected to be in the 1–3 keV range.

In table 3 we give revised peak abundance temperatures and fractions when using our rate coefficients compared to using Pütterich *et al*'s data, spanning 01-like to 46-like. The

Table 3. Comparison of peak abundance temperatures and fractions as calculated using Pütterich *et al*'s data [6], and Pütterich *et al*'s data with 01- to 36-like replaced with our data. The ionisation rate coefficients originate from Loch *et al* [47]. Note $[x] = 10^x$.

Ion-like	Charge	Putt T_{peak}	Putt f_{peak}	This work T_{peak}	This work f_{peak}	$\Delta T\%$	$\Delta f\%$
01-like	W^{73+}	3.88[+9]	0.440	4.06[+9]	0.426	4.72	−3.04
02-like	W^{72+}	2.29[+9]	0.442	2.46[+9]	0.405	7.66	−8.39
03-like	W^{71+}	1.48[+9]	0.360	1.64[+9]	0.363	11.2	0.94
04-like	W^{70+}	9.66[+8]	0.294	1.06[+9]	0.304	9.70	3.41
05-like	W^{69+}	7.17[+8]	0.247	7.67[+8]	0.255	6.97	3.30
06-like	W^{68+}	5.72[+8]	0.218	5.97[+8]	0.228	4.37	4.35
07-like	W^{67+}	4.76[+8]	0.199	4.84[+8]	0.213	1.64	6.70
08-like	W^{66+}	4.03[+8]	0.189	3.98[+8]	0.209	−1.34	10.3
09-like	W^{65+}	3.46[+8]	0.195	3.32[+8]	0.216	−3.79	11.1
10-like	W^{64+}	2.99[+8]	0.214	2.82[+8]	0.229	−5.88	7.03
11-like	W^{63+}	2.60[+8]	0.202	2.43[+8]	0.198	−6.58	−1.75
12-like	W^{62+}	2.25[+8]	0.188	2.11[+8]	0.179	−6.09	−4.99
13-like	W^{61+}	2.01[+8]	0.182	1.89[+8]	0.174	−5.83	−4.33
14-like	W^{60+}	1.80[+8]	0.172	1.70[+8]	0.171	−5.89	−1.00
15-like	W^{59+}	1.62[+8]	0.163	1.52[+8]	0.166	−6.10	1.36
16-like	W^{58+}	1.47[+8]	0.157	1.38[+8]	0.167	−6.31	6.41
17-like	W^{57+}	1.36[+8]	0.139	1.27[+8]	0.154	−6.56	10.5
18-like	W^{56+}	1.26[+8]	0.140	1.16[+8]	0.157	−7.40	12.1
19-like	W^{55+}	1.17[+8]	0.147	1.07[+8]	0.150	−8.22	1.76
20-like	W^{54+}	1.08[+8]	0.150	9.83[+7]	0.160	−9.28	6.65
21-like	W^{53+}	1.01[+8]	0.148	9.01[+7]	0.162	−10.4	9.89
22-like	W^{52+}	9.29[+7]	0.144	8.33[+7]	0.167	−10.4	15.7
23-like	W^{51+}	8.60[+7]	0.143	7.73[+7]	0.153	−10.2	6.79
24-like	W^{50+}	8.01[+7]	0.146	7.14[+7]	0.156	−10.9	6.37
25-like	W^{49+}	7.41[+7]	0.159	6.57[+7]	0.164	−11.3	3.05
26-like	W^{48+}	6.74[+7]	0.181	6.02[+7]	0.174	−10.8	−4.09
27-like	W^{47+}	5.97[+7]	0.136	5.47[+7]	0.182	−8.38	33.6
28-like	W^{46+}	5.10[+7]	0.353	5.03[+7]	0.188	−1.43	−46.8
29-like	W^{45+}	4.32[+7]	0.227	4.62[+7]	0.157	7.16	−30.5
30-like	W^{44+}	3.74[+7]	0.196	4.21[+7]	0.150	12.6	−23.5
31-like	W^{43+}	3.40[+7]	0.194	3.79[+7]	0.177	11.3	−8.90
32-like	W^{42+}	3.22[+7]	0.108	3.30[+7]	0.248	2.45	130
33-like	W^{41+}	3.11[+7]	0.044	2.94[+7]	0.224	−5.47	410
34-like	W^{40+}	3.01[+7]	0.052	2.59[+7]	0.178	−13.9	245
35-like	W^{39+}	2.91[+7]	0.049	2.29[+7]	0.164	−21.5	233
36-like	W^{38+}	2.81[+7]	0.093	2.05[+7]	0.231	−27.2	148
37-like	W^{37+}	2.71[+7]	0.099	1.88[+7]	0.176	−30.4	78.3
38-like	W^{36+}	2.59[+7]	0.118	1.75[+7]	0.157	−32.6	33.9
39-like	W^{35+}	2.45[+7]	0.143	1.63[+7]	0.155	−33.4	8.74
40-like	W^{34+}	2.28[+7]	0.180	1.53[+7]	0.160	−32.6	−11.2
41-like	W^{33+}	2.10[+7]	0.165	1.45[+7]	0.132	−31.0	−19.9
42-like	W^{32+}	1.94[+7]	0.156	1.37[+7]	0.128	−29.4	−18.2
43-like	W^{31+}	1.79[+7]	0.155	1.31[+7]	0.130	−26.7	−15.9
44-like	W^{30+}	1.64[+7]	0.159	1.26[+7]	0.131	−23.5	−17.6
45-like	W^{29+}	1.49[+7]	0.169	1.20[+7]	0.147	−19.9	−12.9
46-like	W^{28+}	1.32[+7]	0.177	1.12[+7]	0.154	−14.9	−13.0

effect on the ionisation balance of replacing the ten $4d$-shell DR rates, 46-like to 37-like are clearly seen between 1 and 2×10^7 K. The extent of the effect of the new rates extends beyond those replaced and is present at the 10^{-3} level up to 28-like (W^{46+}) and down to 53-like (W^{21+}). This accounts for the numerical difference between table 3 in the present work, and table 7 of Preval *et al* [42] for some of the common ionisation stages. Due to the effect on the abundances of adjacent stages because of replacing these rates some caution should be exercised when using the abundances below W^{28+}.

8. Comparison with Pütterich *et al*

The agreement between our total recombination rate coefficients and Pütterich *et al*'s [6] is very poor for all $4d$ ions, with their rates being consistently higher than the present

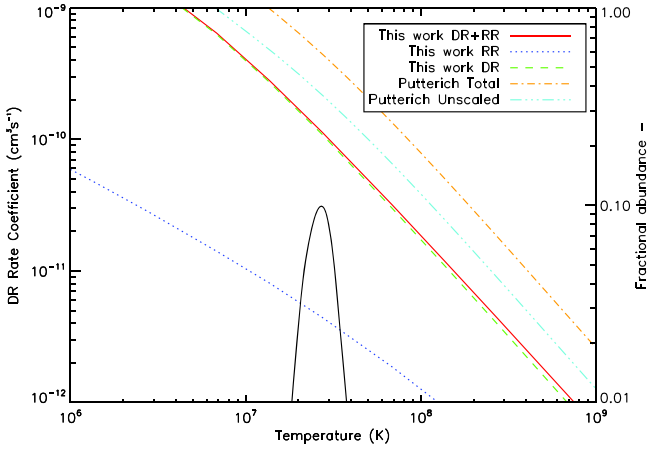

Figure 9. Comparison of the present recombination rate coefficients, split into DR (green-dashed), RR (blue-dotted), and the total of these (solid-red) with Pütterich *et al*'s scaled (orange-dot) and unscaled (cyan-dash triple dot) results for 37-like. The solid black parabola indicates the peak abundance fraction for 37-like.

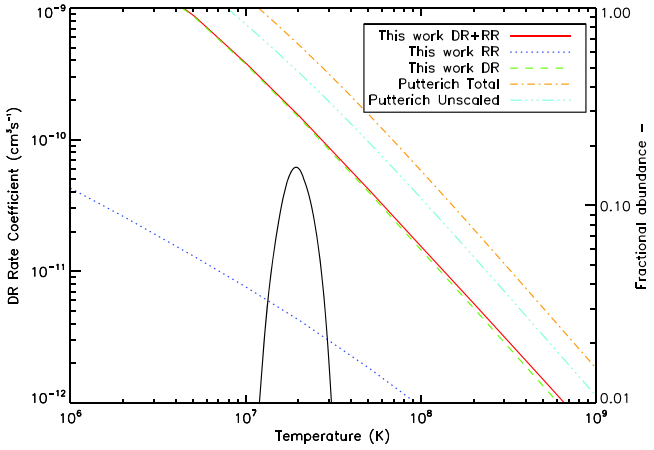

Figure 10. Same as figure 9, but for 42-like.

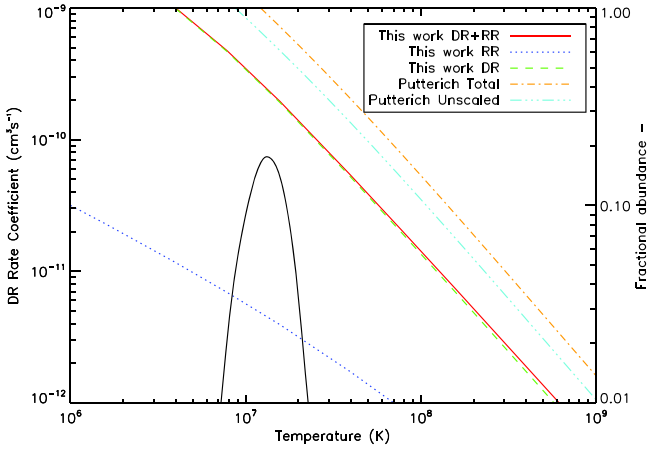

Figure 11. Same as figure 9, but for 46-like.

work. In figures 9–11 we have plotted our total recombination rate coefficients for 37-like, 42-like, and 46-like, respectively, along with Pütterich *et al*'s scaled and unscaled results. The differences between the present work and Pütterich *et al*'s are

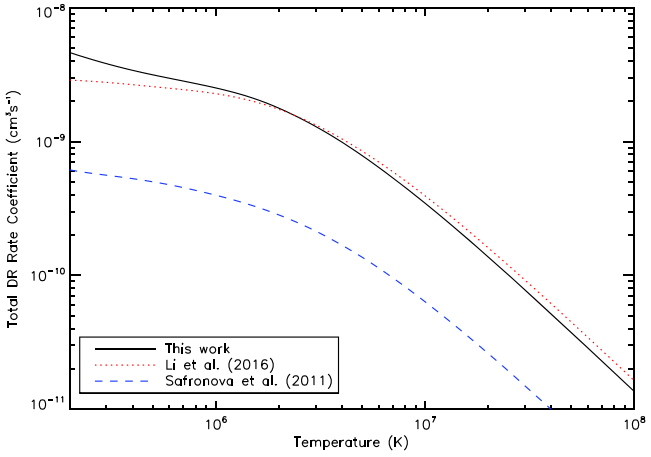

Figure 12. Total DR rate coefficients for 46-like as calculated in the present work (black solid line), by Li *et al* [27] (red dotted line), and by Safronova *et al* [16] (blue-dashed line).

fairly constant. The scaled results are a factor 3–4 larger than the present work at peak abundance temperature, while the unscaled results are a factor 2–2.5 larger.

9. Comparison with other works

Unlike the ionisation states considered in Preval *et al* [48], very few detailed calculations exist for the 4*d*-shell ions of tungsten. To date, detailed calculations have been performed for 37-, 39-, 45-, and 46-like. We compare each of these calculations with the present results.

9.1. 46-like

Like other closed shell ions, 46-like is an important ion for plasma diagnostic purposes. As well as the present work, DR rate coefficients for this ion have been calculated by Safronova *et al* [16] using HULLAC and Li *et al* [27] using FAC. We have plotted the present total DR rate coefficients, along with those calculated by Safronova *et al* and Li *et al* in figure 12. Our and Li *et al*'s DR rate coefficients are in relatively good agreement, differing by ∼0%–10% between $\sim 9 \times 10^5$ and 6×10^6 K. This difference gradually increases to 20% by 1×10^8 K.

Our total DR rate coefficients are consistently larger than Safronova *et al*'s by a factor ∼8 over all temperatures. We note that the DR rate coefficients calculated by Safronova *et al* neglects 4*p* excitations in the *N*- and $(N+1)$-electron targets. However, the contribution from 4*p* alone is not enough to account for the large difference between our and Safronova *et al*'s rate coefficients. We demonstrate this in figure 13, where we have plotted the total DR rate coefficients calculated in CA and IC for the 4–4 core excitation, along with their respective 4*p* and 4*d* contributions. At maximum, 4*p* contributes 15% to the 4–4 CA total at high temperatures, while the rest is provided by 4*d*. Because our results are in relatively good agreement with those calculated by Li *et al*, the large difference between our DR rate coefficients and

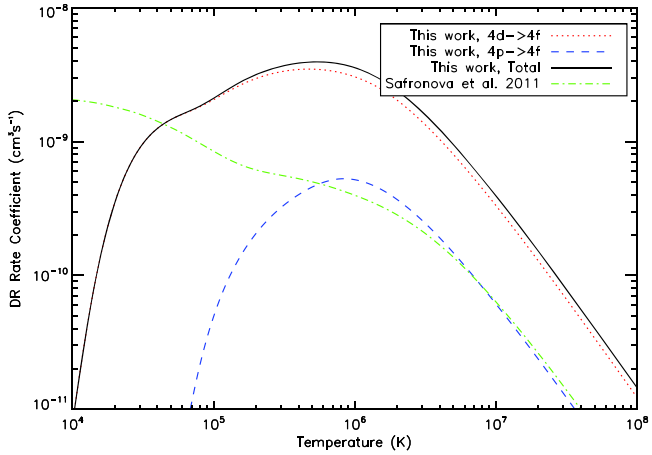

Figure 13. Comparison of total CA DR rate coefficients for the 46-like 4–4 core excitation to the total DR rate coefficients of Safronova *et al* [16]. We also include the constituent 4*d*–4*f* and 4*p*–4*f* contributions to the 4–4 total.

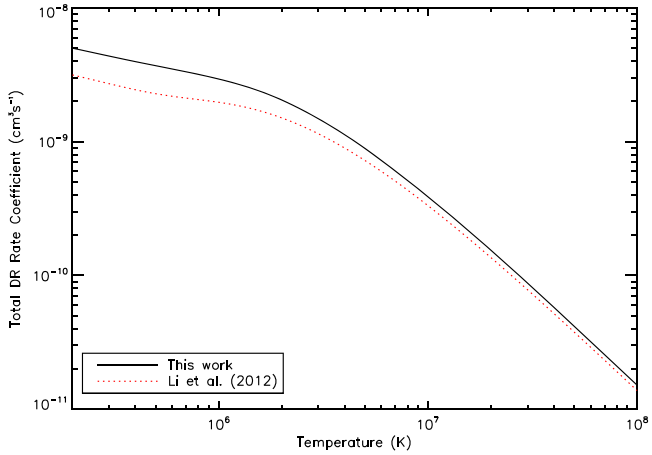

Figure 14. Total DR rate coefficients for 45-like as calculated in the present work (black solid line), and by Li *et al* [25] (red dotted line).

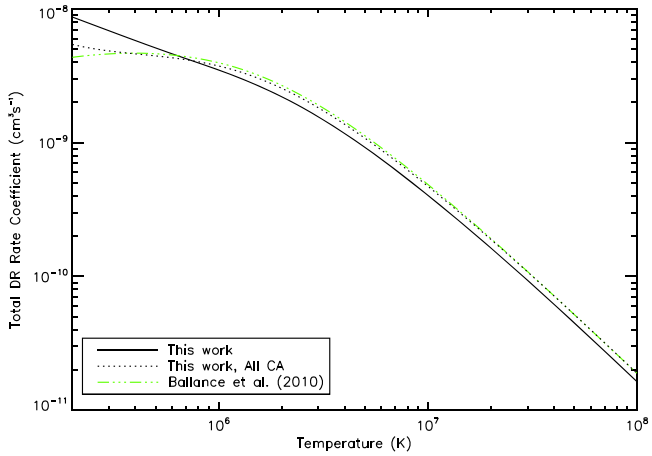

Figure 15. Total DR rate coefficients for 39-like as calculated in the present work (black solid line), and by Ballance *et al* [49] (green triple dotted–dashed line). We also include our CA result for this ion (black dotted line).

Safronova *et al*'s appears to be due to some systematic problem/omission in the authors' calculation.

We note that large differences between our results and Safronova *et al*'s are not limited to the present work. For example, Preval *et al* [41] noted a difference of ∼47% between their work and that of Safronova *et al* [21] for 10-like tungsten. However, comparison of Preval *et al*'s 10-like results with Behar *et al* [24] (calculated with HULLAC) showed differences of $<10\%$. More recently, a calculation by Li *et al* [27] for 10-like showed differences of 30%–40% with Safronova *et al* [21] over a wide temperature range while showing good agreement with Preval *et al* at peak abundance temperature. In addition, Preval *et al* [42] recently compared their calculated 28- and 29-like DR rate coefficients to those presented by Safronova *et al* [15, 18]. As in the previous case, large systematic differences were observed of 27% and a factor 11 for 28- and 29-like, respectively. Excellent agreement was seen between Preval *et al* and Behar *et al* [23] for 28-like with differences of ∼7% at peak abundance temperature. For 29-like, good agreement between Preval *et al* and Kwon *et al* [28] was seen with differences of 23% at peak abundance temperature. Without repeating Safronova *et al*'s calculations (which is beyond the scope of this work), the origin of the aforementioned systematic difference is unknown.

9.2. 45-like

Only one calculation has been done for 45-like tungsten. Li *et al* [25] used FAC to calculate DR rate coefficients for this ion. In figure 14 we have plotted our DR rate coefficients for 45-like, along with Li *et al*'s results. Good agreement is seen over the entire temperature range, with the best agreement seen at high temperatures. At 10^8 K our DR rate coefficients are smaller than Li *et al*'s results, differing by 9%. As we move towards peak abundance temperature (2.9×10^7 K), this difference increases slightly to 11%. The maximum difference between our and Li *et al*'s DR rate coefficients is 40%, occurring at $\sim 10^5$ K. This difference is unlikely to be due to the positioning of resonances at low temperature, as we have previously shown that the DR rate coefficient is insensitive to positioning at threshold.

9.3. 39-like

The only calculation available for 39-like was done by Ballance *et al* [49], who used a CA distorted wave (CADW) code, named DRACULA (Griffin *et al* [50]) to calculate DR for $\Delta n = 0, 1, 2$ processes. In figure 15 we have plotted Ballance *et al*'s calculation, along with our total DR rate coefficient calculated in both IC and CA. The shape of all three curves matches very well from high temperatures down to $\sim 10^6$ K. The present CA results are in near perfect agreement with Ballance *et al*'s, differing by $<0.1\%$ for temperatures $>10^7$ K. As Ballance *et al*'s calculation mirrors ours at high temperature, this shows our result is reliable. The difference between the present IC result and the CADW result is fairly constant between $\sim 10^7$ and 10^8 K, differing

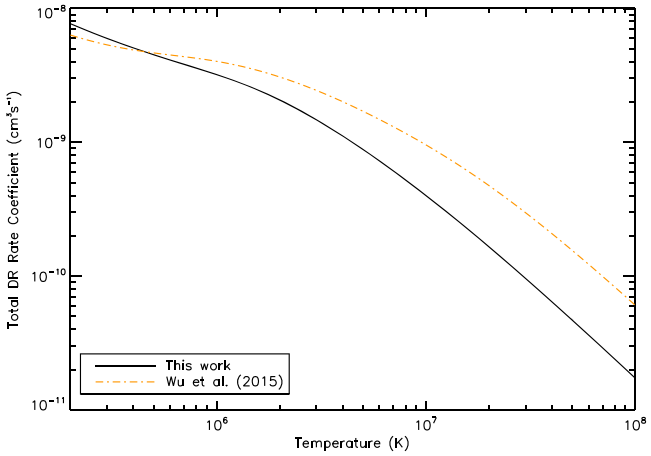

Figure 16. Total DR rate coefficients for 37-like as calculated in the present work (black solid line), and by Wu *et al* [52] (orange-dot-dashed line).

by 15%–16%. Differences between all three curves appear for temperatures $<10^6$ K. It has been shown previously that the low temperature DR rate coefficient in IC is insensitive to resonance positioning due to the density of resonances near threshold. However, in the case of CA, there are far fewer resonances than in IC, meaning that any differences will be dependent upon the quality of the structure calculation.

9.4. 37-like

37-like is the simplest 4*d*-shell ion with only a single 4*d* electron. Interestingly, this ion has been considered twice by Wu *et al* [51, 52]. For the purpose of this comparison, we compare with the results of the latest analysis by the authors, where they calculated DR rate coefficients for 37-like using FAC. In figure 16 we have plotted our total DR rate coefficients for 37-like, along with Wu *et al*'s [52] results. Large differences can be seen between our results and Wu *et al*'s for temperatures $>5 \times 10^5$ K, with the differences gradually getting larger with increasing temperature. At peak abundance temperature, Wu *et al*'s DR rate coefficients are larger than ours by a factor ~3. A similar discrepancy was described in Preval *et al* [48], where other ions considered by Wu *et al* were also much larger than our own results. It was noted that the discrepancy between the two results could be reduced by removing the core-rearrangement configurations from Preval *et al*'s inner shell DR calculations, hence, reducing high temperature Auger suppression. However, as noted earlier, the inner shell DR core excitation 3–4 only contributes 12% at peak abundance, and 14% at higher temperatures, meaning this cannot be the source of the discrepancy. We also note in our calculations that the high temperature DR rate coefficient does not vary much from ion to ion, and we are in close agreement with Ballance *et al* [49] for 39-like.

10. Conclusions

We have presented a series of DR and RR rate coefficient calculations for the 4*d*-shell ions of tungsten spanning 37- to 46-like. The present work is the first consideration of the $4d^q$ ($q = 1$–10) ions of tungsten. The rich level structure of the $4d^q$ ions, particularly for half-open ions, renders the level-resolved DR rate coefficient insensitive to shifts in the ground state energy due to a high density of resonances close to threshold.

Very few detailed calculations were available to compare the present results with. Relatively good agreement was seen between the present work, and the calculations performed by Ballance *et al* [49] for 39-like, and Li *et al* [25] for 45- and 46-like at peak abundance temperature. Very poor agreement was seen between the present work and the calculations performed by Wu *et al* [51] and Safronova *et al* [16]. Unfortunately, it has still not been possible to pin down the reason for the difference between our calculations and Safronova *et al*'s. We found that the present results were consistently smaller than the scaled ADPAK data of Pütterich *et al* [6] by a factor 3–4, and a factor 2–2.5 when compared to the unscaled data.

In terms of practical applications, revision of the 4*d*-shell atomic data has shifted the peak abundance temperatures of these ions to values comparable to the projected pedestal temperature of ITER. This is significant, as it implies the lower ionisation state tungsten ions (most notably the 4*f*-shell ions) may not be as important as the higher ionisation states.

With this paper, only 27 ionisation stages remain to be calculated for *The Tungsten Project*. These stages span the 4*f*-shell, and then continue into the $n = 5$ and $n = 6$ shells. Given the computational difficulty of the 4*f* shell, we opt to next explore the lanthanide series of ions from 61-like to singly-ionized tungsten. We will then complete *The Tungsten Project* with a final paper covering the 4*f* ions of tungsten, from 47- to 60-like.

Acknowledgements

SPP, NRB, and MGOM acknowledge the support of EPSRC grant EP/1021803 to the University of Strathclyde. All data calculated as part of this work are publicly available on the OPEN-ADAS website https://open.adas.ac.uk.

ORCID iDs

S P Preval https://orcid.org/0000-0001-8552-0766

References

[1] Summers H P, Dickson W J, O'Mullane M G, Badnell N R, Whiteford A D, Brooks D H, Lang J, Loch S D and Griffin D C 2006 *Plasma Phys. Control. Fusion* **48** 263–93
[2] Kotschenreuther M, Hatch D R, Mahajan S, Valanju P, Zheng L and Liu X 2017 *Nucl. Fusion* **57** 064001

[3] Snyder P B, Groebner R J, Hughes J W, Osborne T H, Beurskens M, Leonard A W, Wilson H R and Xu X Q 2011 *Nucl. Fusion* **51** 103016
[4] Post D E, Jensen R V, Tarter C B, Grasberger W H and Lokke W A 1977 *At. Data Nucl. Data Tables* **20** 397–439
[5] Post D, Abdallah J, Clark R E H and Putvinskaya N 1995 *Phys. Plasmas* **2** 2328–36
[6] Pütterich T, Neu R, Dux R, Whiteford A D, O'Mullane M G and the ASDEX Upgrade Team 2008 *Plasma Phys. Control. Fusion* **50** 085016
[7] Foster A R 2008 On the behaviour and radiating properties of heavy elements in fusion plasmas *PhD Thesis* University of Strathclyde
[8] Burgess A 1965 *Astrophys. J.* **141** 1588–90
[9] Badnell N R, O'Mullane M G, Summers H P, Altun Z, Bautista M A, Colgan J, Gorczyca T W, Mitnik D M, Pindzola M S and Zatsarinny O 2003 *Astron. Astrophys.* **406** 1151–65
[10] Chung H K, Chen M H, Morgan W L, Ralchenko Y and Lee R W 2005 *High Energy Density Phys.* **1** 3–12
[11] Kwon D H, Lee W, Preval S, Ballance C P, Behar E, Colgan J, Fontes C J, Nakano T, Li B, Ding X, Dong C Z, Fu Y B, Badnell N R, O'Mullane M, Chung H K and Braams B J 2018 *At. Data Nucl. Data Tables* **119** 250–62
[12] Cowan R D 1981 *The Theory of Atomic Structure and Spectra* (*Los Alamos Series in Basic and Applied Sciences*) (Berkeley, CA: University of California Press)
[13] Bar-Shalom A, Klapisch M and Oreg J 2001 *J. Quant. Spectrosc. Radiat. Transfer* **71** 169–88
[14] Safronova U I, Safronova A S and Beiersdorfer P 2012 *J. Phys. B: At. Mol. Opt. Phys.* **45** 085001
[15] Safronova U I and Safronova A S 2012 *Phys. Rev.* A **85** 032507
[16] Safronova U I, Safronova A S, Beiersdorfer P and Johnson W R 2011 *J. Phys. B: At. Mol. Opt. Phys.* **44** 035005
[17] Safronova U I, Safronova A S and Beiersdorfer P 2016 *J. Phys. B: At. Mol. Opt. Phys.* **49** 225002
[18] Safronova U I, Safronova A S and Beiersdorfer P 2015 *Phys. Rev.* A **91** 062507
[19] Safronova U I, Safronova A S and Beiersdorfer P 2012 *Phys. Rev.* A **86** 042510
[20] Safronova U I, Safronova A S and Beiersdorfer P 2009 *J. Phys. B: At. Mol. Opt. Phys.* **42** 165010
[21] Safronova U I, Safronova A S and Beiersdorfer P 2009 *At. Data Nucl. Data Tables* **95** 751–85
[22] Behar E, Peleg A, Doron R, Mandelbaum P and Schwob J L 1997 *J. Quant. Spectrosc. Radiat. Transfer* **58** 449–69
[23] Behar E, Mandelbaum P and Schwob J L 1999 *Eur. Phys. J.* D **7** 157–61
[24] Behar E, Mandelbaum P and Schwob J L 1999 *Phys. Rev.* A **59** 2787–93
[25] Li B W, O'Sullivan G, Fu Y B and Dong C Z 2012 *Phys. Rev.* A **85** 052706
[26] Li M, Fu Y, Su M, Dong C and Koike F 2014 *Plasma Sci. Technol.* **16** 182–7
[27] Li B, O'Sullivan G, Dong C and Chen X 2016 *J. Phys. B: At. Mol. Opt. Phys.* **49** 155201
[28] Kwon D H and Lee W 2016 *J. Quant. Spectrosc. Radiat. Transfer* **170** 182
[29] Kwon D H and Lee W 2016 *J. Quant. Spectrosc. Radiat. Transfer* **179** 98–104
[30] Spruck K *et al* 2014 *Phys. Rev.* A **90** 032715
[31] Badnell N R *et al* 2016 *Phys. Rev.* A **93** 052703
[32] Badnell N R, Ballance C P, Griffin D C and O'Mullane M 2012 *Phys. Rev.* A **85** 052716
[33] Badnell N R 1986 *J. Phys. B: At. Mol. Phys.* **19** 3827
[34] Badnell N R 1997 *J. Phys. B: At. Mol. Opt. Phys.* **30** 1
[35] Badnell N R 2011 *Comput. Phys. Commun.* **182** 1528
[36] Dzuba V A, Flambaum V V, Gribakin G F and Harabati C 2012 *Phys. Rev.* A **86** 022714
[37] Dzuba V A, Flambaum V V, Gribakin G F, Harabati C and Kozlov M G 2013 *Phys. Rev.* A **88** 062713
[38] Berengut J C, Harabati C, Dzuba V A, Flambaum V V and Gribakin G F 2015 *Phys. Rev.* A **92** 062717
[39] Harabati C, Berengut J C, Flambaum V V and Dzuba V A 2017 *J. Phys. B: At. Mol. Opt. Phys.* **50** 125004
[40] Krantz C, Badnell N R, Müller A, Schippers S and Wolf A 2017 *J. Phys. B: At. Mol. Opt. Phys.* **50** 052001
[41] Preval S P, Badnell N R and O'Mullane M G 2016 *Phys. Rev.* A **93** 042703
[42] Preval S P, Badnell N R and O'Mullane M G 2017 *J. Phys. B: At. Mol. Opt. Phys.* **50** 105201
[43] Savin D W *et al* 2002 *ApJS* **138** 337–70
[44] Ali S, Orban I, Mahmood S, Loch S D and Schuch R 2013 *Astron. Astrophys.* **557** A2
[45] Synge J L 1957 *The Relativistic Gas Series in Physics* (Amsterdam: North-Holland)
[46] Badnell N R, Foster A, Griffin D C, Kilbane D, O'Mullane M and Summers H P 2011 *J. Phys. B: At. Mol. Opt. Phys.* **44** 135201
[47] Loch S D, Ludlow J A, Pindzola M S, Whiteford A D and Griffin D C 2005 *Phys. Rev.* A **72** 052716
[48] Preval S P, Barstow M A, Badnell N R, Hubeny I and Holberg J B 2017 *Mon. Not. R. Astron. Soc.* **465** 269–80
[49] Ballance C P, Loch S D, Pindzola M S and Griffin D C 2010 *J. Phys. B: At. Mol. Opt. Phys.* **43** 205201
[50] Griffin D C, Pindzola M S and Bottcher C 1985 *Phys. Rev.* A **31** 568–75
[51] Wu Z, Fu Y, Ma X, Li M, Xie L, Jiang J and Dong C 2015 *Atoms* **3** 474
[52] Wu Z, Zhang Y, Fu Y, Surzhykov A, Fritzsche S and Dong C 2015 *Eur. Phys. J.* D **69** 140